

Nanomagnetic engineering of the properties of domain wall atom traps

T. J. Hayward, A. D. West, K. J. Weatherill, T. Schrefl, I. G. Hughes et al.

Citation: *J. Appl. Phys.* **110**, 123918 (2011); doi: 10.1063/1.3671631

View online: <http://dx.doi.org/10.1063/1.3671631>

View Table of Contents: <http://jap.aip.org/resource/1/JAPIAU/v110/i12>

Published by the [American Institute of Physics](#).

Related Articles

Interplay between intrinsic and stacking-fault magnetic domains in bi-layered manganites
Appl. Phys. Lett. **101**, 132402 (2012)

The Fourier analysis of magnetic force microscopy imaging
J. Appl. Phys. **112**, 063913 (2012)

The magnetic Y-branch nanojunction: Domain-wall structure and magneto-resistance
Appl. Phys. Lett. **101**, 102403 (2012)

Fast domain wall dynamics in MnAs/GaAs films
Appl. Phys. Lett. **101**, 072408 (2012)

Magnetic domain wall induced, localized nanowire reversal
Appl. Phys. Lett. **101**, 062415 (2012)

Additional information on J. Appl. Phys.

Journal Homepage: <http://jap.aip.org/>

Journal Information: http://jap.aip.org/about/about_the_journal

Top downloads: http://jap.aip.org/features/most_downloaded

Information for Authors: <http://jap.aip.org/authors>

ADVERTISEMENT



Special Topic Section:
PHYSICS OF CANCER

Why cancer? Why physics? [View Articles Now](#)

Nanomagnetic engineering of the properties of domain wall atom traps

T. J. Hayward,^{1,a)} A. D. West,² K. J. Weatherill,² T. Schrefl,³ I. G. Hughes,² and D. A. Allwood¹

¹*Department of Materials Science and Engineering, University of Sheffield, Sheffield, United Kingdom*

²*Department of Physics, University of Durham, Durham, United Kingdom*

³*St Pölten University of Applied Sciences, St Pölten, Austria*

(Received 6 September 2011; accepted 18 November 2011; published online 29 December 2011)

We have used the results of micromagnetic simulations to investigate the effects of nanowire geometry and domain wall magnetization structure on the characteristic parameters of magnetic atom traps formed by domain walls in planar ferromagnetic nanowires. It is found that when traps are formed in the near-field of a domain wall both nanowire geometry and wall structure have a substantial effect on trap frequency (how tightly atoms are spatially confined) and adiabaticity (how closely the atoms' magnetic moments track the applied field direction within the trap). We also show that in certain regimes a trap's depth depends only on the amplitude of an externally applied rotating magnetic field, thus allowing it to be tuned independently of the trap's other critical parameters. © 2011 American Institute of Physics. [doi:10.1063/1.3671631]

INTRODUCTION

Contemporary laser cooling techniques allow clouds of atoms to be routinely prepared with temperatures in the micro-Kelvin range. In such conditions, atom clouds represent idealized quantum mechanical systems that not only allow insight into fundamental phenomena, such as the behavior of quantum degenerate matter,^{1,2} but also have great technological potential through the development of matter wave interferometry³ and novel sensors,⁴ and in quantum information processing.^{5,6}

To realize these applications, atom clouds must not only be confined in velocity space, but also trapped physically. This can be achieved using either optical interactions^{7–10} or, for paramagnetic atoms, magnetic interactions.¹¹ In the latter case, atoms are subject to magnetic field gradients created from either current carrying conductors (e.g. Refs. 12–14), or ferromagnetic patterns/microstructures (e.g. Refs. 15–20). The possibility of miniaturizing these systems and integrating them into substrate-bound “atom chips”²¹ makes such approaches extremely attractive for technological applications.

In a previous publication, we have used micromagnetic simulations to demonstrate the feasibility of creating atom traps using the monopole-like magnetic fields emanating from domain walls (DWs) in planar magnetic nanowires.²² These DWs have particle-like properties and can be transported controllably around complex nanowire networks (e.g. Ref. 23). The resulting mobility of atom traps created by such DWs is non-typical for magnetic atom traps based on patterned magnetic microstructures and is extremely attractive for quantum information processing applications. Furthermore, DW atom traps will allow tight confinement of atoms in all three dimensions. Recently we have demonstrated substantial progress toward our goal of experimentally realizing DW atom traps by using an array of DWs in nanowires to create a reconfigurable “atom mirror” Ref. 24.

While we have previously established the basic feasibility of trapping ultra-cold atoms using a DW, the dependence of trap parameters on the specific properties of the nanomagnetic system forming it has not yet been explored. Here we address this issue by using the results of micromagnetic simulations to investigate how the critical parameters of a DW atom trap, namely its depth, frequency, and adiabaticity, depend on both nanowire geometry and the internal magnetization structure of the DW. The direct effects of these parameters are isolated from those due to variation in the DWs' net monopole moment by maintaining a constant nanowire cross-sectional area throughout our calculations.

Our results show that for traps formed above a DW, nanowire geometry substantially alters an atom trap's frequency, adiabaticity, and the maximum obtainable trap depth. We also show that in certain, physically realizable, regimes, the trap depth is dependent only on the magnitude of the externally applied rotating magnetic field that is used to ensure that the trap has a non-zero field minimum. This effectively allows the trap frequency and adiabaticity to be “tuned” independently from the trap depth. In combination, these properties are likely to be useful for designing DW atom traps that can be experimentally realized.

THEORETICAL DESCRIPTION

The magnetic shape anisotropy of a planar nanowire confines its magnetization to lie along its length, and hence DWs represent regions of either converging magnetization (Head-to-Head, H2H) or diverging magnetization (Tail-to-Tail, T2T) (see Fig. 1 (a)). Each DW therefore carries a net monopole moment with effective “magnetic charge” $q = \pm 2 \mu_0 M_s w t$,^{24,25} where M_s is the nanowire's saturation magnetization, w and t are the nanowire's width and thickness, and μ_0 is the permeability of free space. In previous publications,^{25,26} we have shown that the field emanating from a DW can be approximated by assuming that this charge acts

^{a)}Electronic mail: T.Hawyard@sheffield.ac.uk.

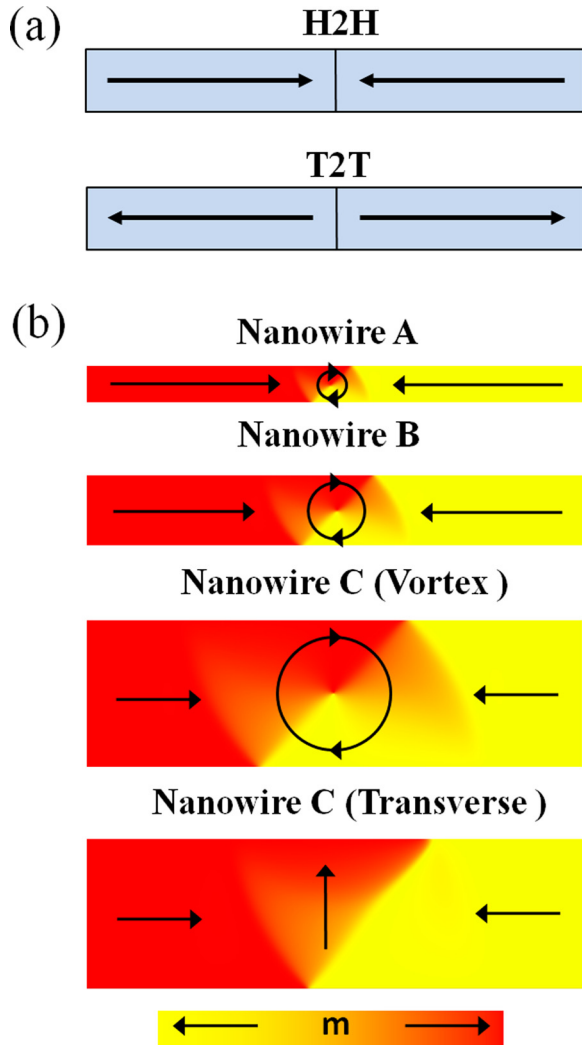


FIG. 1. (Color online) (a) Schematic diagrams of head-to-head (H2H) and tail-to-tail (T2T) domain walls. (b) Micromagnetically simulated domain wall structures for nanowires A–C.

as a point-monopole at the DW center, resulting in the Coulomb-like magnetic field:

$$\mathbf{B}_{\text{DW}}(\mathbf{r}) = \frac{q}{4\pi r^2} \hat{\mathbf{r}} \quad (1)$$

where r is the distance of a point from the DW center. While highly accurate in the far-field, the finite spatial distribution of magnetic poles within the DW causes substantial deviations from this model when considering points closer to the nanowire.²⁶ This spatial distribution is modified as the geometry of the nanowire and DW magnetization structure are altered, leading to the dependence of trap parameters on nanowire geometry that we will present later. In this paper, the point-monopole model will be used to provide the reader with an intuitive picture of how DW atom traps are formed and as a reference through which to understand how the finite spatial distribution of poles within a DW affects the atom trap it creates. From this point onward, \mathbf{B}_{DW} will be used generically to refer to the field from a DW rather than solely that calculated using the point-monopole model.

Figure 2(a) illustrates schematically how a magnetic field with form similar to \mathbf{B}_{DW} can be manipulated to create

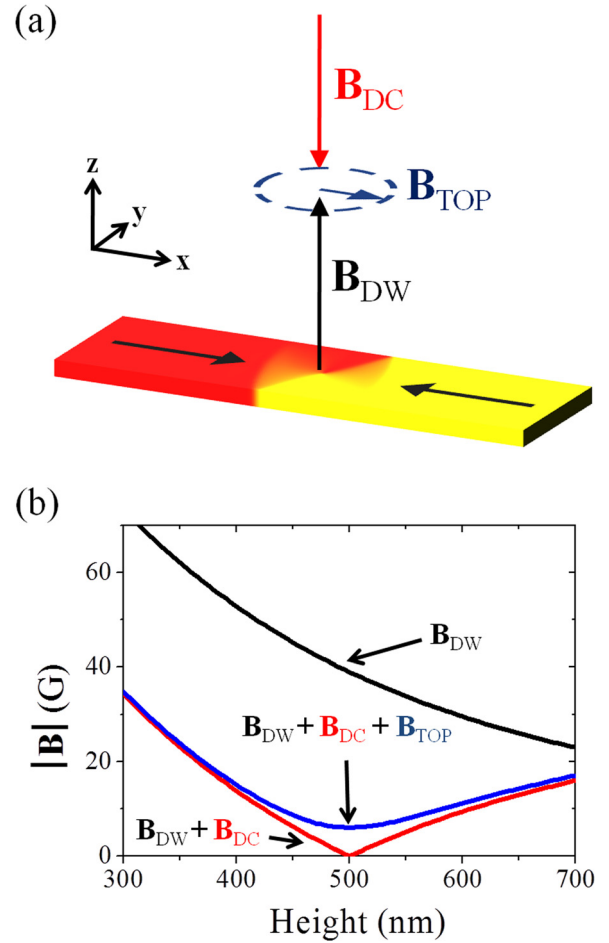


FIG. 2. (Color online) (a) Schematic representation of the experimental geometry required to create a DW atom trap. (b) Plots showing calculated magnetic field as a function of height above a DW in a $\text{Ni}_{80}\text{Fe}_{20}$ nanowire. The plots illustrate how the externally applied fields (\mathbf{B}_{DC} and \mathbf{B}_{TOP}) are combined with \mathbf{B}_{DW} to create an atom trap with a non-zero field minima. Data are shown for Nanowire B ($w=400$ nm, $t=20$ nm) with the trap formed 500 nm above its center. $|\mathbf{B}_{\text{TOP}}| = 6$ G.

an atom trap. A paramagnetic atom moving adiabatically in a magnetic field gradient $\nabla|\mathbf{B}|$ will experience a force $\mathbf{F} = -m_F g_F \mu_B \nabla|\mathbf{B}|$, where m_F is the atom's magnetic quantum number, g_F is the Landé g -factor, and μ_B is the Bohr magneton. Atoms in states where $m_F g_F > 0$ are attracted to minima in the magnetic field and are termed “weak-field-seeking.” In this paper we will consider ^{87}Rb atoms that have been optically pumped into the weak-field-seeking state $z^5S_{1/2} F=2, m_F=2$ ($g_F=1/2$) state.

Because $|\mathbf{B}_{\text{DW}}|$ increases as distance to the DW decreases, in isolation, a DW will simply repel weak-field-seeking atoms. To create a field minimum that may be used to trap atoms, an external magnetic field, \mathbf{B}_{DC} , is applied in opposition to the dominantly z -axis orientated field directly above the DW. At some height, z_{trap} , \mathbf{B}_{DC} exactly cancels \mathbf{B}_{DW} , yielding the required field minimum (Fig. 2(b)).

To achieve tight traps with long lifetimes, it is required that the magnetic field at the trap center, $|\mathbf{B}|_{\text{min}} > 0$. If this criterion is not met, atomic states with different m_F become degenerate at the trap minimum, allowing the atoms to perform Majorana spin flips to untrapped states and being lost from the trap. To overcome this problem, we consider the

time orbiting potential (TOP) approach²⁷ and apply a rotating magnetic field in the x - y plane, $\mathbf{B}_{\text{TOP}}(t)$. Provided that the frequency, ω , of $\mathbf{B}_{\text{TOP}}(t)$ is high enough, the atoms will only experience a time-averaged field landscape with minimum $|\mathbf{B}_{\text{min}}| = |\mathbf{B}_{\text{TOP}}|$.

With the application of \mathbf{B}_{DC} and \mathbf{B}_{TOP} , the instantaneous components of the magnetic field at a time, t , are:

$$\begin{aligned} \mathbf{B}(\mathbf{r}, t) &= \begin{pmatrix} B_x(\mathbf{r}, t) \\ B_y(\mathbf{r}, t) \\ B_z(\mathbf{r}) \end{pmatrix} = \mathbf{B}_{\text{DW}} + \mathbf{B}_{\text{DC}} + \mathbf{B}_{\text{TOP}} \\ &= \mathbf{B}_{\text{DW}} + \begin{pmatrix} 0 \\ 0 \\ |\mathbf{B}_{\text{DC}}| \end{pmatrix} + \begin{pmatrix} |\mathbf{B}_{\text{TOP}}| \cos(\omega t) \\ |\mathbf{B}_{\text{TOP}}| \sin(\omega t) \\ 0 \end{pmatrix} \end{aligned} \quad (2)$$

where \mathbf{B}_{DW} is calculated either from the point monopole model or from more complex analytical²⁶ or numerical²² models of domain wall pole distributions, and ω is the angular frequency of \mathbf{B}_{TOP} . Assuming that the atoms follow the field adiabatically and experience only the time averaged-field, they will then be subject to a magnetic field-landscape defined by:

$$|\mathbf{B}(\mathbf{r})| = \frac{1}{T} \int_0^T |\mathbf{B}(\mathbf{r}, t)| dt \quad (3)$$

where $T = 2\pi/\omega$. This integral does not have an analytic solution even for the simple monopole model, and hence all of the calculations of $|\mathbf{B}(\mathbf{r})|$ presented in this paper were performed numerically. We note that our approach here assumes that the DW remains fixed as \mathbf{B}_{TOP} rotates. In reality, the larger TOP fields considered in this paper might be sufficient to induce DW motion; however, this could be easily prevented by patterning artificial defects into the nanowires.

Having established the basic form of the fields that are used to create a DW atom trap, we now turn attention to the critical parameters that define an atom's interaction with a trap.

The trap depth, U , defines the minimum energy barrier an atom must overcome to escape from an atom trap and therefore has a strong influence on an atom's average lifetime within the trap. In general, the depth of a magnetic atom trap can be calculated using $U = m_{\text{FGF}} \mu_{\text{B}} (|\mathbf{B}|_{\infty} - |\mathbf{B}|_{\text{min}})$, where $|\mathbf{B}|_{\infty}$ is the field far from the DW, outside of the trapping potential. In this paper, we express U as an effective trap temperature $T = \Delta E/k_{\text{B}}$, where k_{B} is Boltzmann's constant.

For DW atom traps $|\mathbf{B}|_{\infty}$ is purely due to the isotropic externally applied fields and hence $|\mathbf{B}|_{\infty} = \sqrt{|\mathbf{B}_{\text{DC}}|^2 + |\mathbf{B}_{\text{TOP}}|^2}$. The trap depth is therefore given by:

$$T_{\infty} = \frac{1}{k_{\text{B}}} m_{\text{FGF}} \mu_{\text{B}} \left(\sqrt{|\mathbf{B}_{\text{DC}}|^2 + |\mathbf{B}_{\text{TOP}}|^2} - |\mathbf{B}_{\text{TOP}}| \right). \quad (4)$$

For a TOP trap, the calculation of trap depth is complicated by the addition of a second route via which the atoms may escape. While \mathbf{B}_{TOP} removes the field-zero at the trap center in the time-averaged field landscape, as it rotates it creates a circle of instantaneous field zeros in the x - y plane below the trap. If an atom encounters this "circle of death," there is a

high chance of it performing a spin-flip to an untrapped state and therefore being lost. By considering that for any point on the circle $\sqrt{B_x(\mathbf{r}, t)^2 + B_y(\mathbf{r}, t)^2} = |\mathbf{B}_{\text{TOP}}|$ and $|B_z(\mathbf{r})| = |\mathbf{B}_{\text{DC}}|$, it can be shown that the time-averaged strength of the magnetic field at any position on the "circle of death" is given by:

$$|\mathbf{B}|_{\text{circle}} = \frac{4|\mathbf{B}_{\text{TOP}}|}{\pi}. \quad (5)$$

The trap depth, T_{circle} , due to this effect is therefore given by:

$$T_{\text{circle}} = m_{\text{FGF}} \mu_{\text{B}} \frac{(4 - \pi)}{\pi k_{\text{B}}} |\mathbf{B}_{\text{TOP}}|. \quad (6)$$

In the preceding, we assume that $|\mathbf{B}(\mathbf{r})|$ always increases consistently along all vectors between the trap center and the "circle of death." We have found that this is the case for all of the traps considered in this paper; however, we observe empirically that for $|\mathbf{B}_{\text{TOP}}| > 2|\mathbf{B}_{\text{DC}}|$, a field maximum may be found prior to reaching the circle. This is likely to affect the trap depth in cases where large values of \mathbf{B}_{TOP} are used or when a trap is formed far from the DW.

In practice, the trap depth is limited by whichever of T_{circle} and T_{∞} is lower. As T_{circle} increases with increasing $|\mathbf{B}_{\text{TOP}}|$, while T_{∞} decreases, the trap depth will be limited by T_{circle} at low $|\mathbf{B}_{\text{TOP}}|$ and by T_{∞} at higher $|\mathbf{B}_{\text{TOP}}|$, with a crossover between the two depths occurring at:

$$|\mathbf{B}_{\text{TOP}}|^{\text{cross}} = \frac{\pi}{\sqrt{(16 - \pi^2)}} |\mathbf{B}_{\text{DC}}|. \quad (7)$$

As T_{circle} is only dependent on the value of $|\mathbf{B}_{\text{TOP}}|$, this leads to the remarkable conclusion that for low values of the TOP field the trap depth is entirely independent of the monopole moment of DW that is used to form the trap. It should be noted that this analysis of T_{circle} was not included in our previous study of DW atom traps.²²

A second important characteristic parameter of an atom trap is the trap frequency, ω_{trap} , which determines the spatial confinement of trapped atoms and also the spacing of energy levels within the trap. Treating the trap as a quantum harmonic oscillator (i.e., a quadratic potential):

$$\omega_i = \sqrt{\frac{\mu_{\text{B}} d^2 |\mathbf{B}|}{m_{\text{A}} dr_i^2}} \quad (8)$$

$$\omega_{\text{trap}} = \sqrt[3]{\omega_x \omega_y \omega_z} \quad (9)$$

where ω_i is the characteristic frequency of the trap along Cartesian axis r_i and m_{A} is the mass of the trapped atom. In general, the potential landscapes created by DW atom traps are not purely quadratic, and hence the value of ω_{trap} best representing the system depends to some degree on the temperature of the trapped atoms. In this paper, we simplify this problem by fitting values of the trap frequency over a fixed distance of ± 100 nm from the trap center. ω_{trap} is a particularly critical parameter for TOP traps, as for trapped atoms to respond to the time-averaged magnetic field, the TOP field

must be rotated at a frequency much greater than the characteristic trap frequency (i.e., $\omega_{\text{trap}} \ll \omega$). This criteria represent a significant consideration in the design of DW atom traps, as creating large time-orbiting fields at high frequencies is technically challenging, particularly in an ultrahigh-vacuum environment.

An important parameter related to ω_{trap} is the trap's adiabaticity, which is defined here as $\omega_L/\omega_{\text{trap}}$, where ω_L is the minimum value of a trapped atom's Larmor frequency as found at the trap center:

$$\omega_L = \frac{\mu_B |\mathbf{B}_{\text{TOP}}|}{\hbar} \quad (10)$$

where \hbar is the reduced Planck's constant. As ω_{trap} effectively describes the rate at which the magnetic field changes in the atom's frame of reference, and ω_L describes the rate at which the atom is able to respond to changes in the field direction, this parameter ultimately dictates whether or not the atom's magnetic moment can follow the trap's varying magnetic field adiabatically. Thus, for successful trapping:

$$\frac{\omega_L}{\omega_{\text{trap}}} \gg 1. \quad (11)$$

METHOD

To investigate how the critical parameters of DW atom traps depend on nanowire geometry, we consider three 8.4 μm long $\text{Ni}_{80}\text{Fe}_{20}$ nanowires with differing widths (w) and thicknesses (t): Nanowire A: ($w = 200$ nm, $t = 40$ nm), Nanowire B: ($w = 400$ nm, $t = 20$ nm), Nanowire C: ($w = 800$ nm, $t = 10$ nm). As all three nanowires have the same cross-sectional area, the total monopole moment of their DWs will be identical, and hence any difference between the traps they create is solely due to the spatial distribution of magnetic poles within the DWs.

Physically appropriate DW structures were generated by relaxing simple bi-domain magnetization configurations in accordance with the Landau–Lifshitz–Gilbert equation using a proprietary finite-element micromagnetic code.²⁸ Standard parameters were used to represent the material parameters of $\text{Ni}_{80}\text{Fe}_{20}$ (saturation magnetization, $M_S = 860$ kA/m, exchange stiffness, $A = 13$ pJ/m, magnetocrystalline anisotropy constant, $K_1 = 0$). A characteristic mesh size of 5 nm was used in the regions of the nanowires containing the DWs, while larger 20 nm meshes were used in uniformly magnetized regions. In all three nanowire geometries, vortex DW structure²⁹ was energetically favored, although in Nanowire C, this was bistable with transverse DW structure, allowing the effect of DW magnetization structure on trap parameters to be investigated. Micromagnetically simulated DW structures for all three nanowires are shown in Fig. 1(b).

For each nanowire, \mathbf{B}_{DW} was calculated from the quasi-static Maxwell equations using a finite element/boundary element method.³⁰ Calculations were performed across regular meshes (cell size ≤ 20 nm) that extended at least ± 200 nm from the trap center in each direction and were also large enough to fully contain the “circle of death” for a

given value of $|\mathbf{B}_{\text{TOP}}|$. The magnetic fields created by the nanowires' end domains were subtracted from \mathbf{B}_{DW} by considering point-monopole charges of magnitude $-q/2$ placed at the nanowires' ends.

In our calculations, we consider traps formed at $z_{\text{trap}} = 500$ nm, 1000 nm, and 1500 nm with values of $|\mathbf{B}_{\text{TOP}}|$ between 2 and 10 G. $|\mathbf{B}(\mathbf{r})|$ was calculated by first adding an appropriate value of \mathbf{B}_{DC} to \mathbf{B}_{DW} so as to create a field minimum at the desired height and then numerically integrating Eq. (3) across 50 time steps to simulate the TOP field-landscape. In each time step, the position of the instantaneous field-zero created by \mathbf{B}_{TOP} was located, so as to allow $\mathbf{B}_{\text{circle}}$ to be found. T_{circle} was then calculated using Eq. (6). T_{∞} was calculated using Eq. (4). Trap frequencies were estimated by performing quadratic fits to $|\mathbf{B}(\mathbf{r})|$ along lines extending ± 100 nm from the trap center and then using Eq. (8).

RESULTS AND DISCUSSION

To illustrate the basic variation of trap depth, trap frequency, and adiabaticity with z_{trap} and $|\mathbf{B}_{\text{TOP}}|$, we initially present calculations for atom traps formed using Nanowire B ($w = 400$ nm, $t = 20$ nm) (Fig. 3).

Figure 3(a) shows the calculated variation of trap depth with $|\mathbf{B}_{\text{TOP}}|$ and z_{trap} . It can be seen that for $z_{\text{trap}} = 500$ nm and 1000 nm, the trap depth is limited by T_{circle} for all values of $|\mathbf{B}_{\text{TOP}}|$ and hence increases linearly in accordance with Eq. (6). That T_{circle} is the critical parameter here can be understood by considering Fig. 3(d), which plots the value of $|\mathbf{B}_{\text{DC}}|$ required to form a trap as a function of z_{trap} . For $z_{\text{trap}} = 500$ nm and 1000 nm, the required values of $|\mathbf{B}_{\text{DC}}|$ are 39 G and 12 G, respectively, leading to values of $|\mathbf{B}_{\text{TOP}}|^{\text{cross}}$ of 49 G and 15 G. As these values are outside of the range $|\mathbf{B}_{\text{TOP}}|$ modeled, the trap depth is always limited by T_{circle} . In contrast to this, for $z_{\text{trap}} = 1500$ nm, $|\mathbf{B}_{\text{DC}}| = 5.6$ G, and hence $|\mathbf{B}_{\text{TOP}}|^{\text{cross}} = 7.1$ G, leading to a transition from T_{circle} to T_{∞} within the calculated data. Consequently, the trap depth increases linearly to a maximum ~ 127 μK and then decreases in accordance with Eq. (4). In the calculated data, the cross-over between T_{circle} and T_{∞} occurs at a slightly higher value of $|\mathbf{B}_{\text{TOP}}|$ than is predicted by Eq. (7) (indicated by dashed line). This is due to the finite discretization of the regular mesh, which results in a slight error in the calculated value of $|\mathbf{B}|_{\text{circle}}$.

In Fig. 4, we illustrate how the position of the “circle of death” is modified by changing the value of $|\mathbf{B}_{\text{TOP}}|$. It is observed that as $|\mathbf{B}_{\text{TOP}}|$ increases, the circle adopts a larger radius and descends toward the DW. This evolution can be understood by considering the monopole-like field pattern generated by the DW along with the condition that for any point on the circle, the in-plane component of \mathbf{B}_{DW} must be equal in magnitude to \mathbf{B}_{TOP} , while the z-component must be equal and opposite to \mathbf{B}_{DC} : Considering points in an x-y plane containing the trap center, the magnitude of the in-plane magnetic field ($\sqrt{B_x(\mathbf{r}, t)^2 + B_y(\mathbf{r}, t)^2}$) increases with distance from the trap center. Hence as $|\mathbf{B}_{\text{TOP}}|$ increases, the circle must adopt a larger radius. However, this increase in the in-plane field is associated with a decrease in $B_z(\mathbf{r})$, and thus the circle must simultaneously descend toward the DW to maintain a z-component equal and opposite to \mathbf{B}_{DC} .

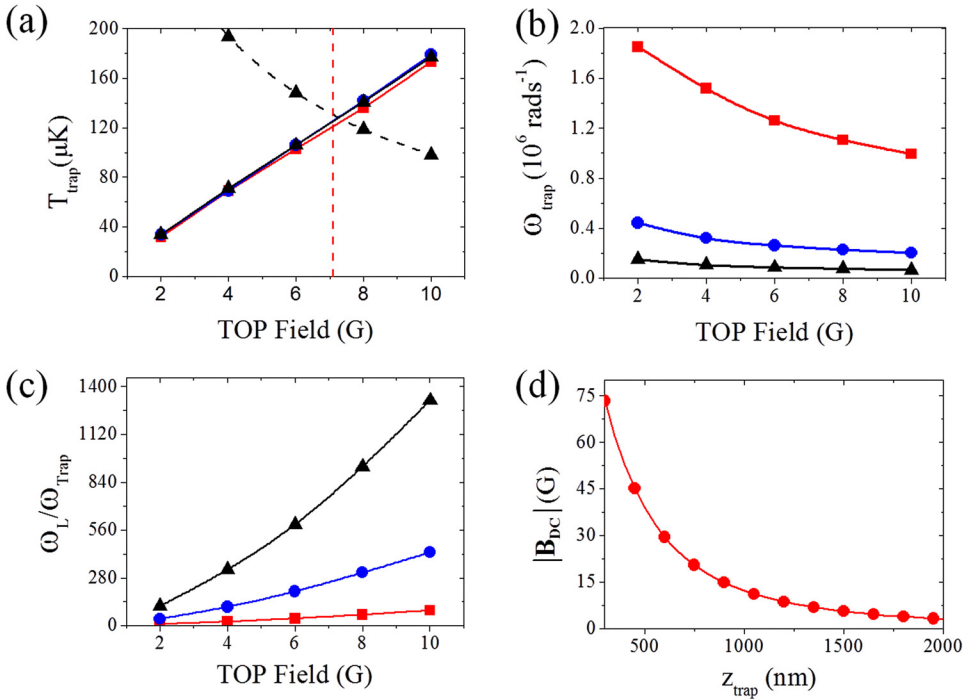


FIG. 3. (Color online) Calculated values of (a) trap depth, (b) trap frequency, and (c) adiabaticity as a function of $|\mathbf{B}_{\text{TOP}}|$ for Nanowire B ($w=400$ nm, $t=20$ nm). Data are shown for $z_{\text{trap}}=500$ nm (squares), 1000 nm (circles), and 1500 nm (triangles). In (a), full lines represent T_{circle} while dashed lines represent T_{∞} . (d) Value of $|\mathbf{B}_{\text{DC}}|$ required to create a trap as a function of z_{trap} .

Figure 3(b) plots the variation of ω_{trap} with $|\mathbf{B}_{\text{TOP}}|$. For all trap heights, ω_{trap} decreases as $|\mathbf{B}_{\text{TOP}}|$ increases, approximately halving over the range of TOP fields studied. This trend reflects the manner in which the addition of the TOP field “smooths” the time-averaged field landscape, resulting in more gently varying field gradients (Fig. 5(a)). Varying the trap height produces an even stronger variation of trap frequency. For example, with $|\mathbf{B}_{\text{TOP}}| = 6$ G, a trap formed at $z_{\text{trap}} = 500$ nm has a trap frequency of $1.26 \times 10^6 \text{ rads}^{-1}$, while under the same conditions, a trap at $z_{\text{trap}} = 1500$ nm has a trap frequency of only $8.89 \times 10^4 \text{ rads}^{-1}$, over an order of magnitude lower. This variation is the result of the rapid decrease in $d^2|\mathbf{B}(\mathbf{r})|/dr_i^2$ with height above the DW (Fig. 5(b)).

Figure 3(c) illustrates the variation of the trap’s adiabaticity as $|\mathbf{B}_{\text{TOP}}|$ is varied. This variation is found to be stronger than that of ω_{trap} because the decrease of ω_{trap} with $|\mathbf{B}_{\text{TOP}}|$ is complemented by a simultaneous linear increase in

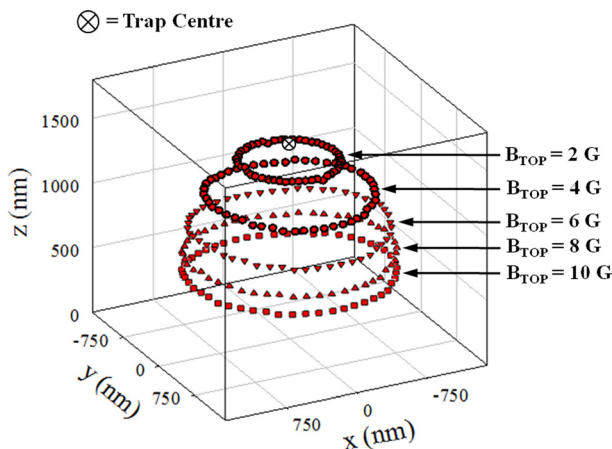


FIG. 4. (Color online) Evolution of the “circle of death” as $|\mathbf{B}_{\text{TOP}}|$ is varied. Data are shown for Nanowire B with $z_{\text{trap}} = 1500$ nm.

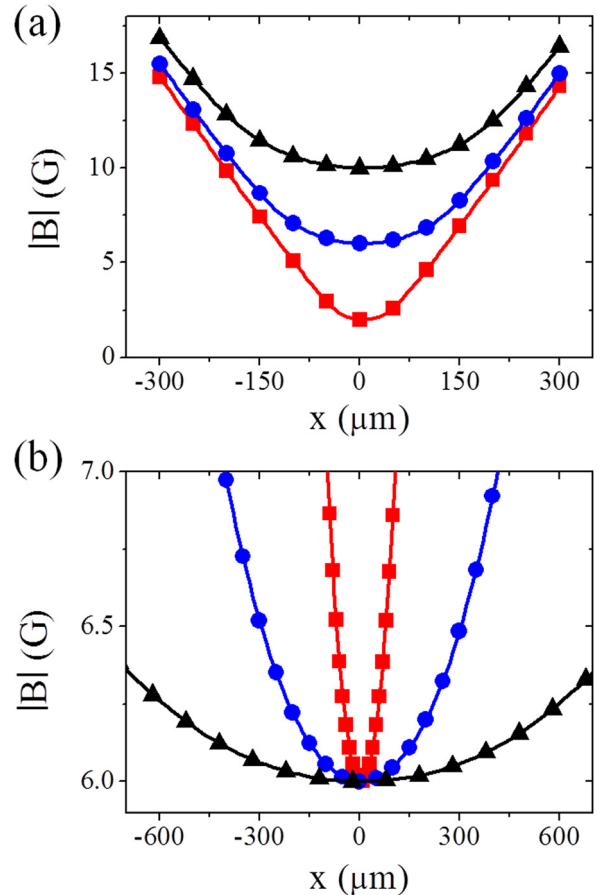


FIG. 5. (Color online) (a) Variation of $|\mathbf{B}|$ with x position for Nanowire B with $z_{\text{trap}} = 1500$ nm. Data are shown for $|\mathbf{B}_{\text{TOP}}| = 2$ G (squares), 6 G (circles), and 10 G (triangles). (b) Variation of $|\mathbf{B}|$ with x position for Nanowire B with $|\mathbf{B}_{\text{TOP}}| = 6$ G. Data are shown for $z_{\text{trap}} = 500$ nm (squares), 1000 nm (circles), and 1500 nm (triangles).

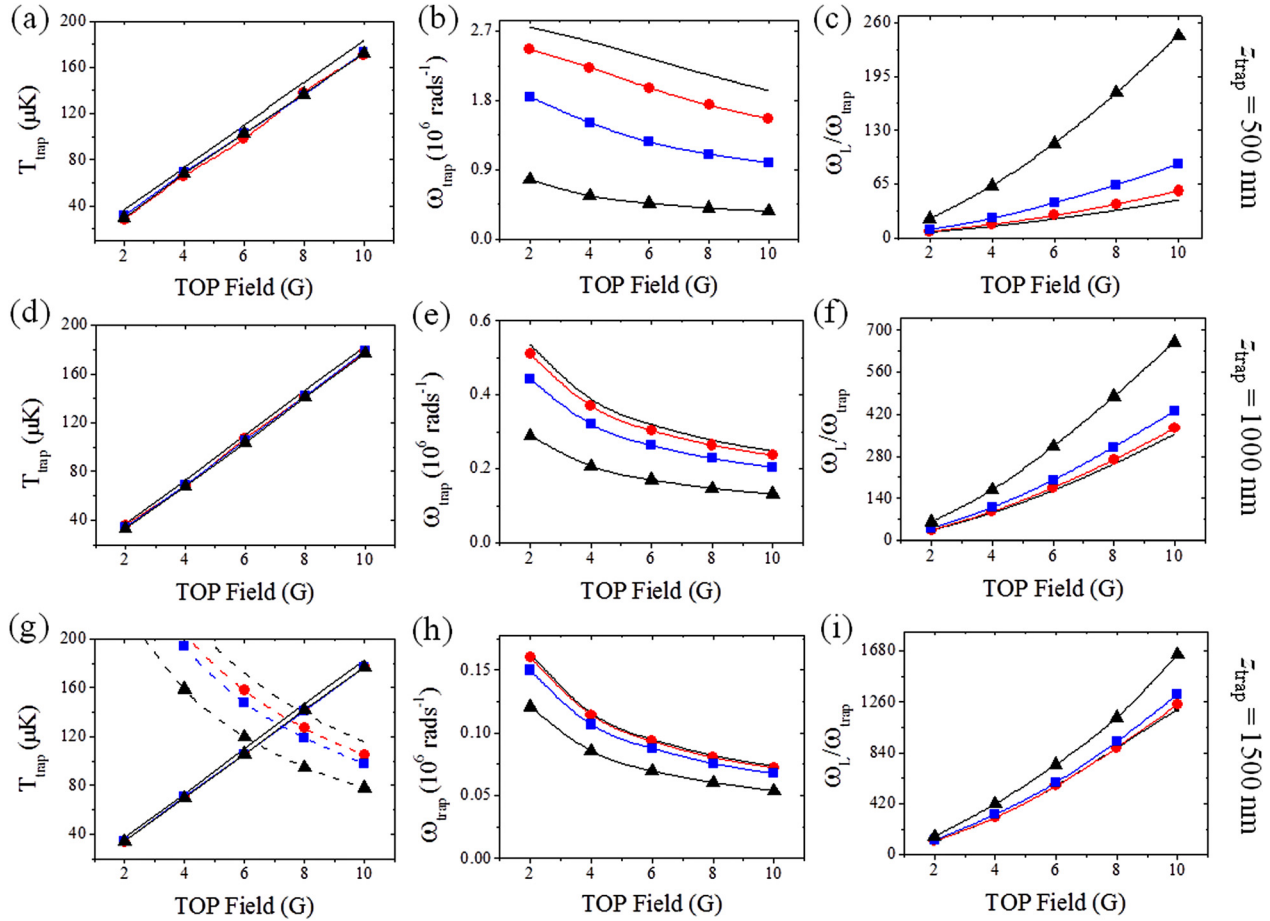


FIG. 6. (Color online) Variation of trap depth, frequency, and adiabaticity with nanowire geometry. Data are shown for Nanowires A (circles), B (squares), and C (triangles) as well as for the point-monopole model (no symbols). (a) to (c) $z_{\text{trap}} = 500$ nm. (d) to (f) $z_{\text{trap}} = 1000$ nm. (g) to (i) $z_{\text{trap}} = 1500$ nm. In (a), (d), and (g), full lines represent T_{circle} while dashed lines represent T_{∞} .

ω_L . In combination, these features allow the adiabaticity to be altered by several orders of magnitude even with the limited range of values of $|\mathbf{B}_{\text{TOP}}|$ we consider here. The adiabaticity also decreases dramatically as z_{trap} increases. However, this is solely due changes in ω_{trap} , as ω_L depends only on $|\mathbf{B}_{\text{TOP}}|$ (Eq. 10).

We now turn our attention to the effect of nanowire geometry and DW structure on trap parameters.

Figures 6(a), 6(d), and 6(g) compare calculated values of the trap depth for Nanowires A–C with those from the point monopole model. As in the calculations for Nanowire B discussed earlier, for $z_{\text{trap}} = 500$ nm and 1000 nm, the trap depth is limited by T_{circle} in the modeled parameter range. Hence, the trap depth depends only on $|\mathbf{B}_{\text{TOP}}|$ and is independent of the nanowire dimensions (the slight differences between the data at $z_{\text{trap}} = 500$ nm are again the result of finite mesh discretization). At $z_{\text{trap}} = 1500$ nm, a transition between T_{circle} and T_{∞} is again seen. Here distinct geometry dependence is observed with $|\mathbf{B}_{\text{TOP}}|^{\text{cross}}$ occurring at lower $|\mathbf{B}_{\text{TOP}}|$ for wider nanowires. Figure 7 illustrates the reason for this: The finite pole distributions in the micromagnetically simulated nanowires lead to reduced magnetic fields at a given height in comparison to the point-monopole model.²⁶ This difference grows as the nanowires' widths increase due to the pole-distributions becoming more extended. Thus,

lower values of $|\mathbf{B}_{\text{DC}}|$ are required to create the trap, and $|\mathbf{B}_{\text{TOP}}|^{\text{cross}}$ is consequently reduced. In regimes where T_{∞} dominates, the trap depth is also lower for wider nanowires as the reduced value of $|\mathbf{B}_{\text{DC}}|$ leads to lower values of $|\mathbf{B}_{\infty}|$. An important conclusion here is that for a given trap height and DW charge, nanowire geometry ultimately determines the maximum trap depth that may be obtained.

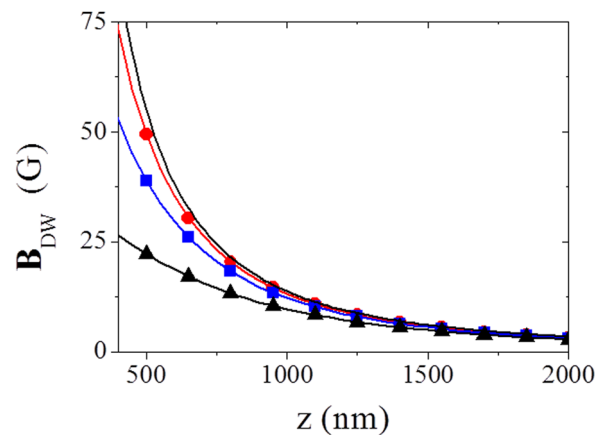


FIG. 7. (Color online) Variation of $|\mathbf{B}_{\text{DW}}|$ with height above center of DW. Data are shown for Nanowires A (circles), B (squares), and C (triangles) as well as for the point-monopole model (no symbols).

Figures 6(b), 6(e), and 6(h) present calculated values of ω_{trap} for all three nanowire geometries. Decreasing the width of the nanowire can be seen to increase the trap frequency for given height and TOP field, with the point monopole model representing an upper limit of what may be obtained for given DW charge. At $z_{\text{trap}} = 500$ nm, a substantial effect is observed, with Nanowire A producing traps with frequencies $\sim 300\%$ higher than those created by Nanowire C, while at greater values of z_{trap} , the differences between the three geometries are less pronounced. The origin of these effects lies in the fact that in the near-field, more extended pole distributions result in more slowly varying field gradients than more concentrated pole distributions. Moving toward the far-field, the effects of an extended pole distribution become less relevant, resulting in the convergence of the curves toward that of the point-monopole. The reader may also note an apparent “flattening” of the curves at low $|\mathbf{B}_{\text{TOP}}|$ when $z_{\text{trap}} = 500$ nm. This is due to the non-harmonic shape of the trapping potential: Under these conditions, the field landscape shows notable deviations from quadratic form over the fitted data range (± 100 nm).

Figures 6(c), 6(f), and 6(i) illustrate how the atom traps’ adiabaticity is modified by nanowire geometry. As ω_L is independent of nanowire geometry, the observed variation is entirely due to the variation of ω_{trap} described in the previous paragraph. Thus the adiabaticity increases with increasing

nanowire width with this dependence becoming less significant at larger trap heights.

Having discussed the effect of nanowire geometry we now discuss how the internal magnetization structure of a DW affects the parameters of an atom trap. As is well known, planar magnetic nanowires support two basic types of DWs (Ref.29): the “transverse” form, in which the magnetization of the DW lies perpendicular to the nanowire length, and the “vortex” form where the DW magnetization rotates around a nanoscopic “core” of out-of-plane magnetization. As indicated earlier in the paper, vortex DW structure is energetically favorable in all three of the modeled nanowire geometries; however, Nanowire C will also support a meta-stable transverse DW configuration (Fig. 1(b)). Studying traps in this nanowire therefore allows the effects of DW magnetization structure to be isolated from those due to total DW charge and nanowire geometry. The results of calculations comparing the characteristic parameters of traps formed by the two DW geometries can be found in Fig. 8.

The basic effect of DW structure can be understood by considering that moving from a vortex to a transverse DW effectively compresses the DW pole distribution. The result of this is that transverse walls produce traps with higher values of $|\mathbf{B}_{\text{TOP}}|^{\text{cross}}$, T_{∞} , and ω_{trap} and lower values of adiabaticity than an equivalent vortex wall. A further noticeable effect is that with transverse DWs, traps are no longer

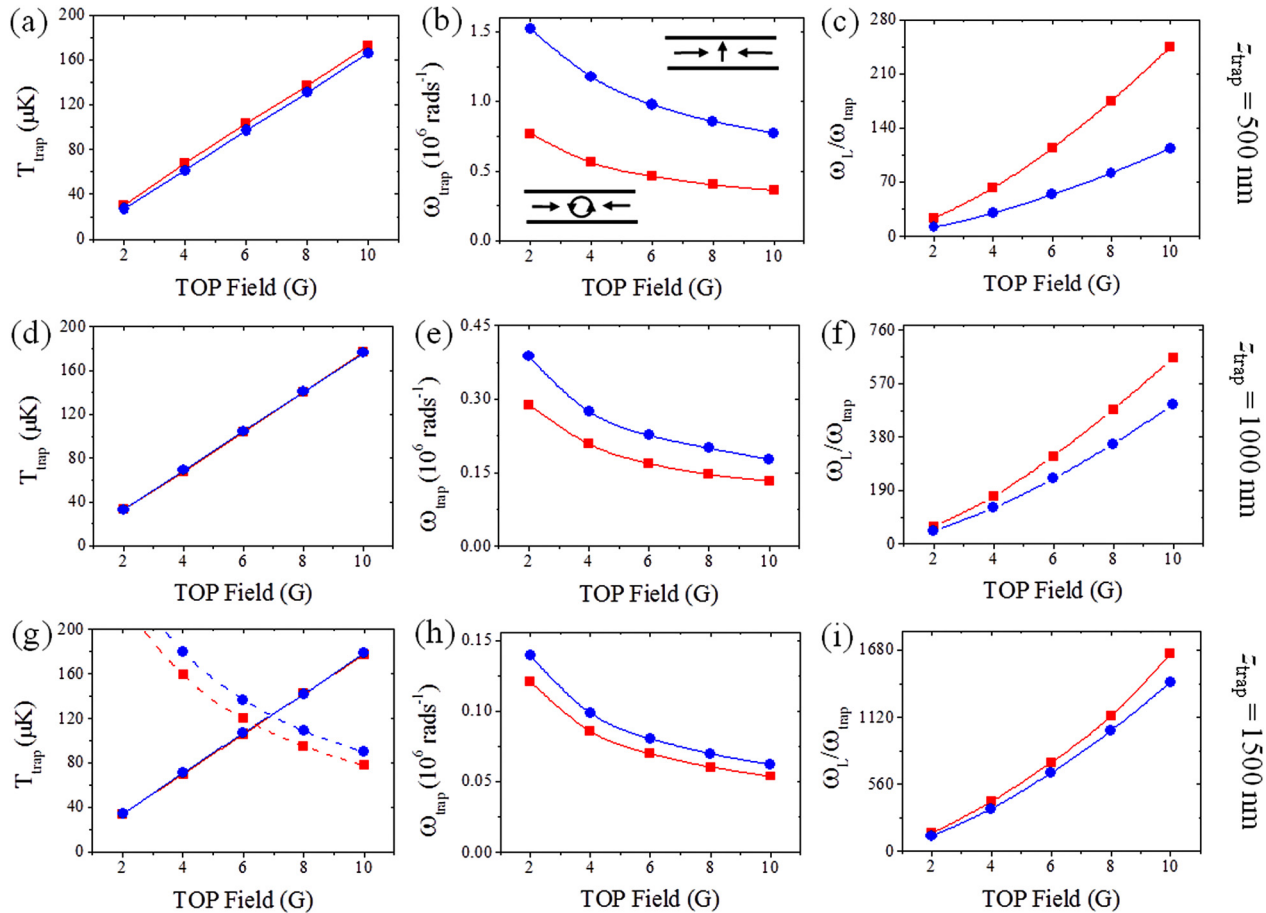


FIG. 8. (Color online) Comparison between the parameters of traps formed by a vortex DW (squares) and a transverse DW (circles) in Nanowire C. (a) to (c) $z_{\text{trap}} = 500$ nm. (d) to (f) $z_{\text{trap}} = 1000$ nm. (g) to (i) $z_{\text{trap}} = 1500$ nm. In (a), (d), and (g), full lines represent T_{circle} while dashed lines represent T_{∞} .

formed above the center of the nanowire as they are for vortex DWs but are displaced ~ 200 nm toward the edge of the nanowire. This reflects the symmetry of the triangular transverse DW structure, which, as we have shown previously,^{26,31} results in an offset in the position of the effective center of the DWs charge distribution.

CONCLUSIONS

In this study, the results of micromagnetic simulations have been used to investigate the effect of nanowire geometry and DW magnetization structure on the critical parameters of atom traps formed using DWs in planar magnetic nanowires.

Our results indicate that when considering traps in the near field of a DW (i.e. $z_{\text{trap}} \sim w$), nanowire geometry has a substantial effect on both trap frequency and adiabaticity and also modifies the maximum obtainable trap depth. For given total DW monopole moment, the adiabaticity increases with nanowire width, while the trap frequency and maximum depth decrease. These effects can be understood by a broadening of the DW charge distributions as nanowire width increases. As the height of a trap is increased toward the far-field, the effect of nanowire geometry becomes less pronounced due to the field from the DW's charge distribution tending toward the limiting case of that from a point-monopole.

We have also observed differences between traps formed by transverse and vortex walls in a nanowire of the same geometry. For given trap height and DW monopole moment, a transverse DW wall produces a trap with a higher maximum depth and frequency, and a lower adiabaticity, than a trap formed by a vortex DW in the same nanowire. Again, these effects become less important as the trap height increases.

While nanowire geometry and DW structure will undoubtedly be useful tools in optimizing trap properties, perhaps a more significant result of this work is the observation that for certain regimes of external parameters the trap depth depends only on the magnitude of the TOP field and is therefore independent of nanowire geometry, DW magnetization structure, total DW monopole moment, and trap height. The upshot of this is that these parameters may be used together to "tune" a trap's frequency and adiabaticity while maintaining an experimentally appropriate trap depth. Particularly exciting is the ability to use the trap height in this way due to the strong dependence of trap frequency and adiabaticity upon it. For example, simply by varying nanowire geometry and trap height within the limited ranges considered in this paper, both trap frequency and adiabaticity can be tuned by more than an order of magnitude while maintaining a trap depth in excess of $100 \mu\text{K}$.

In combination, the effects we describe in this paper are likely to be extremely useful in the design and

optimization of DW atom traps that can be experimentally realized.

ACKNOWLEDGMENTS

The authors thank the Engineering and Physical Sciences Research Council for financial support (Grant Nos. EP/F024886/1 and EP/F025459/1).

- ¹M. H. Anderson, J. R. Ensher, M. R. Matthews, C. E. Wieman, and E. A. Cornell, *Science* **269**, 198 (1995).
- ²B. DeMarco and D. S. Jin, *Science* **285**, 1703 (1999).
- ³C. S. Adams, M. Sigel, and J. Mlynek, *Phys. Rep.* **240**, 143 (1994).
- ⁴A. Peters, K. Y. Chung, and S. Chu, *Nature (London)* **400**, 849 (1999).
- ⁵M. A. Nelson and I. L. Chuang, *Quantum Computation and Quantum Information* (Cambridge University Press, Cambridge, UK, 2000).
- ⁶M. Saffman, T. G. Walker, and K. Molmer, *Rev. Mod. Phys.* **82**, 2313 (2010).
- ⁷A. Hemmerich and T. W. Hänsch, *Phys. Rev. Lett.* **70**, 410 (1993).
- ⁸V. I. Balykin, V. S. Letokhov, Yu. B. Ovchinnikov, and A. I. Sidorov, *Phys. Rev. Lett.* **60**, 2137 (1988).
- ⁹M. A. Kasevich, D. S. Weiss, and S. Chu, *Opt. Lett.* **15**, 607 (1990).
- ¹⁰H. F. Hess, G. P. Kochanski, J. M. Doyle, N. Masuhara, D. Kleppner, and T. J. Greytak, *Phys. Rev. Lett.* **59**, 672 (1987).
- ¹¹E. A. Hinds and I. G. Hughes, *J. Phys. D* **32**, R119 (1999).
- ¹²J. Fortágh, A. Grossman, C. Zimmermann, and T. W. Hänsch, *Phys. Rev. Lett.* **81**, 5310 (1998).
- ¹³J. Reichel, W. Hänsel, and T. W. Hänsch, *Phys. Rev. Lett.* **83**, 3398 (1999).
- ¹⁴W. Hänsel, P. Hommelhoff, T. W. Hänsch, and J. Reichel, *Nature* **413**, 498 (2001).
- ¹⁵T. J. Davies, *J. Opt. B: Quantum Semiclassical Opt.* **1**, 408 (1999).
- ¹⁶A. I. Sidorov, R. J. McLean, F. Scharnberg, D. S. Gough, T. J. Davies, B. J. Sexton, G. I. Opat, and P. Hannaford, *Acta Phys. Polonica B* **33**, 2137 (2002).
- ¹⁷S. Eriksson, F. Rairez-Martinez, E. A. Curtis, B. E. Sauer, P. W. Nutter, E. W. Hill, and E. A. Hinds, *Appl. Phys. B* **79**, 811 (2004).
- ¹⁸J. Y. Wang, S. Whitlock, F. Scharnberg, D. S. Gough, A. I. Sidorov, R. J. McLean, and P. Hannaford, *J. Phys. D* **38**, 4015 (2005).
- ¹⁹C. D. J. Sinclair, E. A. Curtis, I. Llorente Garcia, J. A. Retter, B. V. Hall, S. Eriksson, B. E. Sauer, and E. A. Hinds, *Phys. Rev. A* **72**, 031603(R) (2005).
- ²⁰S. Whitlock, R. Gerritsma, T. Fernholz, and R. J. C. Spreeuw, *New J. Phys.* **11**, 023021 (2009).
- ²¹J. Reichel and V. Vuletic, *Atom Chips* (Wiley, New York, 2011).
- ²²D. A. Allwood, T. Schrefl, G. Hrkac, I. G. Hughes, and C. S. Adams, *Appl. Phys. Lett.* **89**, 014102 (2006).
- ²³D. A. Allwood, G. Xiong, C. C. Faulkner, D. Atkinson, D. Petit, and R. P. Cowburn, *Science* **309**, 1688 (2005).
- ²⁴T. J. Hayward, A. D. West, K. J. Weatherill, P. J. Curan, P. W. Fry, P. M. Fundi, M. R. J. Gibbs, T. Schrefl, C. S. Adams, I. G. Hughes, S. J. Bending, and D. A. Allwood, *J. Appl. Phys.* **108**, 043906 (2010).
- ²⁵T. J. Hayward, M. T. Bryan, P. W. Fry, P. M. Fundi, M. R. J. Gibbs, M.-Y. Im, P. Fischer, and D. A. Allwood, *Appl. Phys. Lett.* **96**, 052502 (2010).
- ²⁶A. D. West, T. J. Hayward, K. J. Weatherill, T. Schrefl, D. A. Allwood, and I. G. Hughes, "A simple model for calculating magnetic nanowire domain wall fringe fields," (unpublished).
- ²⁷W. Petrich, M. H. Anderson, J. R. Ensher, and E. A. Cornell, *Phys. Rev. Lett.* **74**, 3352 (1995).
- ²⁸See <http://www.firmasuess.at> for more information on FEMME micromagnetics packages.
- ²⁹R. D. McMichael and M. J. Donahue, *IEEE Trans. Magn.* **33**, 4167 (1997).
- ³⁰T. Schrefl, M. E. Schabes, D. Suess, and M. Stehno, *IEEE Trans. Magn.* **40**, 2341 (2004).
- ³¹T. J. Hayward, M. T. Bryan, P. W. Fry, P. M. Fundi, M. R. J. Gibbs, D. A. Allwood, M.-Y. Im, and P. Fischer, *Phys. Rev. B* **81**, 020410, (2010).